Chapter 1

Derivation of a Cell-Based Mathematical Model of Excitable Cells

Karoline Horgmo Jæger[1] and Aslak Tveito[1,2]

Abstract Excitable cells are of vital importance in biology, and mathematical models have contributed significantly to understand their basic mechanisms. However, classical models of excitable cells are based on severe assumptions that may limit the accuracy of the simulation results. Here, we derive a more detailed approach to modeling that has recently been applied to study the electrical properties of both neurons and cardiomyocytes. The model is derived from first principles and opens up possibilities for studying detailed properties of excitable cells. We refer to the model as the EMI model because both the extracellular space (E), the cell membrane (M) and the intracellular space (I) are explicitly represented in the model, in contrast to classical spatial models of excitable cells. Later chapters of the present text will focus on numerical methods and software for solving the model. Also, in the next chapter, the model will be extended to account for ionic concentrations in the intracellular and extracellular spaces.

1.1 Introduction

Mathematical modeling has a great potential for increasing our understanding of the physiological processes underlying the function of the body. For example, modeling of the electrical properties of excitable cells may provide insight into the complex electrical signaling involved in a number of important functions, like transfer of information through neurons and coordination of the pumping of the heart. A popular model of the conduction of electrical signals in neurons is the so-called cable equation (30), whereas the extracellular potential surrounding neurons is often modeled using the point-source or line-source approximations (6). The three aforementioned models

[1]Simula Research Laboratory, Norway
[2]Department of Informatics, University of Oslo, Norway

A. Tveito et al. (eds.), *Modeling Excitable Tissue*, Simula SpringerBriefs on Computing 7, https://doi.org/10.1007/978-3-030-61157-6_1

have been used extensively to gain insight into the function of neurons and the interpretation of measurements of the extracellular potential around neurons (6; 5; 12). Correspondingly, the conduction of electrical signals through the heart is traditionally modeled using the homogenized bidomain and monodomain models (20). These models are also widely used and have, for instance, provided insight into mechanisms of cardiac arrhythmias (26; 33).

However, despite the success of the above-mentioned classical models of excitable cells, the models have certain shortcomings that may make them inaccurate or impractical in some situations. For example, in the derivation of the cable equation, the extracellular potential is often assumed to be constant (30; 15). Therefore, changes in the extracellular potential generated by the neuron itself or by neighboring neurons (i.e., ephaptic effects) are ignored in the model. This could potentially lead to inaccuracies (16; 2; 34). In addition, the point-source and line-source approximations rely on the assumption that the extracellular space is infinite and homogeneous. Consequently, the models might not be well-suited to interpret extracellular potentials measured when large measurement electrodes are present in the extracellular space close to the neurons (3).

Moreover, the bidomain and monodomain models represent cardiac tissue in a homogenized manner, assuming that the intracellular space, the extracellular space and the cell membrane exist everywhere in the tissue. Because the geometry of the individual cells is not represented, it is very hard to use the models to study the effect of, e.g., the cell geometry or a non-uniform distribution of ion channels on the cell membrane. These properties are both believed to influence cardiac conduction, but their exact effects are not fully understood and call for further investigations (28; 21). In addition, it has been proposed that ephaptic coupling between cardiac cells might occur at small extracellular clefts located at the intercalated discs between cells (29). Since the geometry of the extracellular space is not represented in the homogenized models, it is difficult to use these models to study such ephaptic effects.

In order to account for the difficulties related to the classical models, alternative electrophysiological models have been developed (e.g., (28; 31; 24)). In this chapter, we consider one of these alternative models, referred to as the EMI model, because it explicitly represents the extracellular space (E), the cell membrane (M) and the intracellular space (I). This model has been used to study both neurons (1; 34; 3) and cardiac tissue (32; 31; 18). Because the model represents the extracellular space, the membrane and the intracellular space in a coupled manner, the model allows for representation of ephaptic effects between neurons (34) or cardiomyocytes (18). In addition, since the geometry of the extracellular space is explicitly represented, the model allows for representation of non-homogeneous extracellular surroundings (3). Furthermore, since the geometry of each cell is represented, the model allows for study of the effect of cell geometry and non-uniform distributions of ion channels on cardiac conduction properties (18).

In other words, the EMI model allows for a more detailed representation of excitable cells and tissues than classical models of computational electrophysiology. In fact,

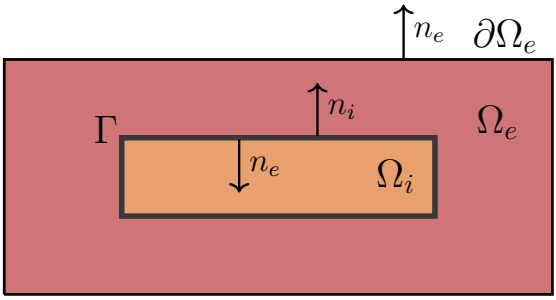

Fig. 1.1: Illustration of an EMI model domain consisting of an extracellular domain, Ω_e, a cell membrane, Γ, and an intracellular domain, Ω_i.

the classical models mentioned above can be derived from the more detailed EMI model by introducing certain simplifying assumptions, see e.g., (1; 8; 11). In this chapter, however, we focus on deriving the EMI model from Maxwell's equations of electromagnetism.

1.2 Derivation of the EMI Model

In this section, we present a derivation of the EMI model for excitable cells. This derivation is to a large extent based on the derivation found in (1; 17). We consider a domain separated into an extracellular part, Ω_e and an intracellular part, Ω_i, like illustrated in Figures 1.1 and 1.3. The cell membrane, denoted by Γ, is defined as the boundary between Ω_i and Ω_e. Here, we derive a model for the electrical potentials in both a domain with a single cell (Figure 1.1) and in a domain with two cells connected at an intercalated disc denoted by $\Gamma_{1,2}$ (Figure 1.3).

1.2.1 Fundamental Equations

We base the derivation of the EMI model on two of the quasi-static approximations of Maxwell's equations, i.e.,

$$\nabla \times \mathbf{E} = 0, \tag{1.1}$$

$$\nabla \times \mathbf{H} = \mathbf{J}. \tag{1.2}$$

Here, $\mathbf{E}$ is the electric field (typically in μF/cm), $\mathbf{H}$ is the magnetic field (typically in μA/cm) and $\mathbf{J}$ is the density of free currents (typically in μA/cm^2). In the quasi-static approximation of (1.2), it is assumed that free unbalanced charges are instantly balanced. The assumptions hold in the intracellular and extracellular spaces. However, we assume that charges may accumulate at the cell membrane and at the intercalated discs between cells. Therefore, we let (1.2) at these locations be replaced by the corresponding equation without the quasi-static approximation, i.e., by

$$\nabla \times \mathbf{H} = \mathbf{J} + \varepsilon \frac{\partial \mathbf{E}}{\partial t}, \tag{1.3}$$

where ε is the permittivity of the medium (typically in μF/cm). In addition, we assume that Ohm's law applies in the intracellular and extracellular domains. This means that

$$\mathbf{J} = \sigma \mathbf{E}, \tag{1.4}$$

where σ is the conductivity of the considered medium (typically in mS/cm). We also note that (1.1) implies that $\mathbf{E}$ is a conservative vector field and that it therefore can be defined as the gradient of a scalar field (9). More specifically, we can define

$$\mathbf{E} = -\nabla u, \tag{1.5}$$

where the scalar u is the electric potential (typically in mV).

1.2.2 Model for the Intracellular and Extracellular Domains

In order to derive equations for the intracellular and extracellular domains, we take the divergence of both sides of (1.2) and apply the vector identity $\nabla \cdot (\nabla \times \mathbf{H}) = 0$, which holds for any vector $\mathbf{H}$ (9). This yields

$$\nabla \cdot \mathbf{J} = 0.$$

Inserting (1.4) and (1.5), we obtain the Laplace equation

$$\nabla \cdot \sigma \nabla u = 0. \tag{1.6}$$

More specifically, for the intracellular and extracellular domains, we have

$$\nabla \cdot \sigma_i \nabla u_i = 0 \quad \text{in } \Omega_i, \tag{1.7}$$

$$\nabla \cdot \sigma_e \nabla u_e = 0 \quad \text{in } \Omega_e, \tag{1.8}$$

where σ_i and σ_e are the intracellular and extracellular conductivities, respectively, and u_i and u_e are the electric potentials in the intracellular and extracellular domains, respectively.

1.2.3 Model for the Membrane

In order to derive the EMI model equations for the membrane, we consider a volume element, B, intersected by the membrane. This volume element may be divided into an extracellular part, B_e, and an intracellular part, B_i, such that $B_e \cup B_i = B$ and $B_e \cap B_i = \emptyset$, as illustrated in Figure 1.2A. In each of these domains, we assume that (1.3) holds. Taking the divergence of both sides of (1.3) and applying the vector identity $\nabla \cdot (\nabla \times \mathbf{H}) = 0$ results in

$$\nabla \cdot \mathbf{J} = -\nabla \cdot \varepsilon \frac{\partial \mathbf{E}}{\partial t}. \tag{1.9}$$

Integrating this equation over each of the volume elements B_i and B_e, we get

$$\int_{B_i} \nabla \cdot \mathbf{J}\, dV = -\int_{B_i} \nabla \cdot \varepsilon \frac{\partial \mathbf{E}}{\partial t}\, dV,$$
$$\int_{B_e} \nabla \cdot \mathbf{J}\, dV = -\int_{B_e} \nabla \cdot \varepsilon \frac{\partial \mathbf{E}}{\partial t}\, dV,$$

and applying the divergence theorem (see e.g., (9)), we obtain

$$\int_{\partial B_i} \mathbf{J} \cdot \mathbf{n}_{B_i}\, dS = -\int_{\partial B_i} \varepsilon \frac{\partial \mathbf{E}}{\partial t} \cdot \mathbf{n}_{B_i}\, dS, \tag{1.10}$$
$$\int_{\partial B_e} \mathbf{J} \cdot \mathbf{n}_{B_e} dS = -\int_{\partial B_e} \varepsilon \frac{\partial \mathbf{E}}{\partial t} \cdot \mathbf{n}_{B_e}\, dS. \tag{1.11}$$

Here, $\mathbf{n}_{B_i}$ and $\mathbf{n}_{B_e}$ are the outward pointing normal vectors of B_i and B_e, respectively. Furthermore, in (1.10) and (1.11), the left-hand side terms represent the free ionic current and the right-hand side terms represent the capacitive current.

1.2.3.1 Ionic Current

We start by considering the left-hand side of (1.10), representing the ionic current. Here, we note that the boundary ∂B_i may be split into two parts, Γ_B and $\partial B_i \setminus \Gamma_B$, where Γ_B is the part of ∂B_i coinciding with the membrane and $\partial B_i \setminus \Gamma_B$ is the remaining part (see Figure 1.2A). We can then write

$$\int_{\partial B_i} \mathbf{J} \cdot \mathbf{n}_{B_i}\, dS = \int_{\partial B_i \setminus \Gamma_B} \mathbf{J} \cdot \mathbf{n}_{B_i}\, dS + \int_{\Gamma_B} \mathbf{J} \cdot \mathbf{n}_i\, dS, \tag{1.12}$$

where $\mathbf{n}_i$ is the outward pointing normal vector of the membrane and $\mathbf{n}_{B_i}$ is the outward pointing normal vector of the remaining part of B_i, as illustrated in Figure 1.2A. At the membrane, the current density, $\mathbf{J}$, consists of currents through different types of ion channels, pumps and exchangers located at the membrane. This current den-

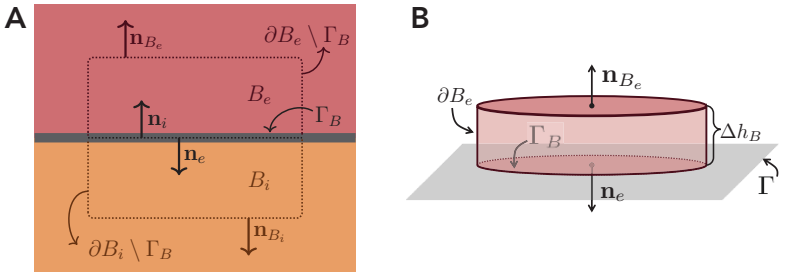

Fig. 1.2: **A**: Illustration of a volume element, B, intersected by the membrane. The volume element is separated into an intracellular part, B_i, and an extracellular part, B_e. **B**: Illustration of a small volume element, B, located on the extracellular part of the membrane.

sity is typically denoted by I_{ion} and given in units of $\mu\text{A/cm}^2$. By convention, I_{ion} is defined to be positive for a flux of positive ions out of the cell (i.e., in the direction of $\mathbf{n}_i$). This gives

$$\int_{\Gamma_B} \mathbf{J} \cdot \mathbf{n}_i \, dS = \int_{\Gamma_B} I_{\text{ion}} \, dS. \tag{1.13}$$

The boundary $\partial B_i \setminus \Gamma_B$ is located in the intracellular domain. Here, we assume that the current density, $\mathbf{J}$, is given by Ohm's law (1.4), such that

$$\int_{\partial B_i \setminus \Gamma_B} \mathbf{J} \cdot \mathbf{n}_{B_i} \, dS = \int_{\partial B_i \setminus \Gamma_B} \sigma_i \mathbf{E} \cdot \mathbf{n}_{B_i} \, dS. \tag{1.14}$$

Inserting (1.13) and (1.14) into (1.12), we get

$$\int_{\partial B_i} \mathbf{J} \cdot \mathbf{n}_{B_i} \, dS = \int_{\partial B_i \setminus \Gamma_B} \sigma_i \mathbf{E} \cdot \mathbf{n}_{B_i} \, dS + \int_{\Gamma_B} I_{\text{ion}} \, dS, \tag{1.15}$$

and similar arguments for the extracellular part of the membrane yield

$$\int_{\partial B_e} \mathbf{J} \cdot \mathbf{n}_{B_e} \, dS = \int_{\partial B_e \setminus \Gamma_B} \sigma_e \mathbf{E} \cdot \mathbf{n}_{B_e} \, dS - \int_{\Gamma_B} I_{\text{ion}} \, dS. \tag{1.16}$$

Note that the negative sign in front of the last term is due to the fact that $\mathbf{n}_e = -\mathbf{n}_i$.

1.2.3.2 Capacitive Current

For the right-hand side part of (1.10), representing the capacitive current, we again split the integral into two parts

$$\int_{\partial B_i} \varepsilon \frac{\partial \mathbf{E}}{\partial t} \cdot \mathbf{n}_{B_i}\, dS = \int_{\partial B_i \setminus \Gamma_B} \varepsilon \frac{\partial \mathbf{E}}{\partial t} \cdot \mathbf{n}_{B_i}\, dS + \int_{\Gamma_B} \varepsilon_\Gamma \frac{\partial \mathbf{E}}{\partial t} \cdot \mathbf{n}_i\, dS.$$

Here, ε_Γ is the permittivity of the membrane. Following the quasi-static assumptions, we assume that the term $\varepsilon \frac{\partial \mathbf{E}}{\partial t}$ is negligible for the part of ∂B_i that does not coincide with the membrane. Furthermore, from (1.5), we get $\mathbf{E} \cdot \mathbf{n}_i = -\nabla u \cdot \mathbf{n}_i \approx v/d$, where

$$v = u_i - u_e \tag{1.17}$$

is the membrane potential and d is the thickness of the membrane. We assume that the membrane can be treated as a capacitor formed by two parallel plates separated by an insulator. In that case, the membrane capacitance per area is given by $C_m = \varepsilon_\Gamma / d$ (13). Therefore,

$$\int_{\partial B_i} \varepsilon \frac{\partial \mathbf{E}}{\partial t} \cdot \mathbf{n}_{B_i}\, dS = \int_{\Gamma_B} \varepsilon_\Gamma \frac{\partial \mathbf{E}}{\partial t} \cdot \mathbf{n}_i\, dS = \int_{\Gamma_B} \frac{\varepsilon_\Gamma}{d} \frac{\partial v}{\partial t}\, dS = \int_{\Gamma_B} C_m \frac{\partial v}{\partial t}\, dS. \tag{1.18}$$

Similar arguments for the extracellular side yield

$$\int_{\partial B_e} \varepsilon \frac{\partial \mathbf{E}}{\partial t} \cdot \mathbf{n}_{B_e}\, dS = -\int_{\Gamma_B} C_m \frac{\partial v}{\partial t}\, dS, \tag{1.19}$$

where the change of sign again is due to the fact that $\mathbf{n}_e = -\mathbf{n}_i$.

1.2.3.3 Collecting the Ionic and Capacitive Currents

Collecting the ionic and capacitive currents by inserting (1.15)–(1.16) and (1.18)–(1.19) into (1.10)–(1.11), we obtain

$$\int_{\partial B_i \setminus \Gamma_B} \sigma_i \mathbf{E} \cdot \mathbf{n}_{B_i}\, dS + \int_{\Gamma_B} I_{\text{ion}}\, dS = -\int_{\Gamma_B} C_m \frac{\partial v}{\partial t}\, dS,$$
$$\int_{\partial B_e \setminus \Gamma_B} \sigma_e \mathbf{E} \cdot \mathbf{n}_{B_e}\, dS - \int_{\Gamma_B} I_{\text{ion}}\, dS = \int_{\Gamma_B} C_m \frac{\partial v}{\partial t}\, dS,$$

which can be rewritten to

$$\int_{\partial B_i \setminus \Gamma_B} \sigma_i \mathbf{E} \cdot \mathbf{n}_{B_i}\, dS = -\int_{\Gamma_B} I_m\, dS, \tag{1.20}$$
$$\int_{\partial B_e \setminus \Gamma_B} \sigma_e \mathbf{E} \cdot \mathbf{n}_{B_e}\, dS = \int_{\Gamma_B} I_m\, dS, \tag{1.21}$$

where the total membrane current density I_m is defined as

$$I_m = C_m \frac{\partial v}{\partial t} + I_{\text{ion}}. \tag{1.22}$$

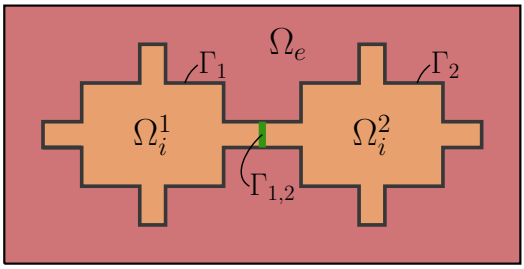

Fig. 1.3: Illustration of an EMI model domain consisting of two cells, Ω_i^1 and Ω_i^2, connected at an intercalated disc, $\Gamma_{1,2}$ and surrounded by an extracellular domain, Ω_e

We now wish to rewrite (1.20)–(1.21) to a differential form. We note that we can divide any volume element, B, intersecting the membrane into a purely intracellular, a purely extracellular, and a membrane intersecting part. We also know that (1.7)–(1.8) hold in the purely intracellular and extracellular parts. Therefore, we are interested in equations (1.20)–(1.21) as the size of B approaches zero. For example, we may consider a small extracellular volume element shaped as a cylinder, as illustrated in Figure 1.2B. As the height, Δh_B, of this cylinder approaches zero, the integral over $\partial B_e \setminus \Gamma_B$ approaches the integral over Γ_B, and we therefore get

$$\int_{\partial B_e \setminus \Gamma_B} \sigma_e \mathbf{E} \cdot \mathbf{n}_{B_e} \, dS \approx \int_{\Gamma_B} \sigma_e \mathbf{E} \cdot \mathbf{n}_{B_e} \, dS.$$

Inserting this approximation into (1.21), we obtain

$$\int_{\Gamma_B} \sigma_e \mathbf{E} \cdot \mathbf{n}_{B_e} \, dS = \int_{\Gamma_B} I_m \, dS \qquad \Rightarrow \qquad \sigma_e \mathbf{E} \cdot \mathbf{n}_{B_e} = I_m,$$

and inserting (1.5) and $\mathbf{n}_e = -\mathbf{n}_{B_e}$, we get

$$\sigma_e \nabla u_e \cdot \mathbf{n}_e = I_m. \tag{1.23}$$

Similar arguments for the intracellular part of the membrane yield

$$-\sigma_i \nabla u_i \cdot \mathbf{n}_i = I_m, \tag{1.24}$$

where the negative sign is due to the negative sign in (1.20). Finally, combining (1.23) and (1.24), we obtain

$$\sigma_e \nabla u_e \cdot \mathbf{n}_e = -\sigma_i \nabla u_i \cdot \mathbf{n}_i = I_m, \tag{1.25}$$

where $I_m = C_m \frac{\partial v}{\partial t} + I_{\text{ion}}$ and $v = u_i - u_e$ (see (1.22) and (1.17)).

1.2.4 Model for the Intercalated Disc

In some cases, we wish to model cells that are connected to each other, as illustrated in Figure 1.3. We then let the intercalated discs connecting the cells be represented as boundaries between the intracellular domains, like the membrane is a boundary between the intracellular and extracellular domains. Furthermore, we assume that the intercalated disc have capacitive properties like the membrane, and that gap junctions allow for currents between neighboring cells, in the same manner as ion channels allows for currents between the intracellular and extracellular spaces. Therefore, the derivation of equations for an intercalated disc follows the exact same lines as the derivation of the membrane equations. More precisely, for two connected cells, we define an intercalated disc potential, w, by

$$w = u_i^1 - u_i^2, \tag{1.26}$$

where u_i^1 and u_i^2 are the electric potentials in Ω_i^1 and Ω_i^2, respectively. In addition, we define a total intercalated disc current density, $I_{1,2}$, by

$$I_{1,2} = C_{1,2}\frac{\partial w}{\partial t} + I_{\text{gap}}, \tag{1.27}$$

where I_{gap} is the current density through the gap junctions, with positive direction in the direction from Ω_i^1 to Ω_i^2, $C_{1,2}$ is the capacitance of the intercalated disc, and $C_{1,2}\frac{\partial w}{\partial t}$ is the capacitive current density of the intercalated disc. Furthermore, following the same arguments as for the derivation of the membrane equations, we end up with an analogue to (1.25) of the form

$$\sigma_i^2 \nabla u_i^2 \cdot \mathbf{n}_i^2 = -\sigma_i^1 \nabla u_i^1 \cdot \mathbf{n}_i^1 = I_{1,2}, \tag{1.28}$$

representing the total current density across the interface.

1.2.5 Models of the Ionic Currents

Mathematical models of the ionic currents governing the membrane potential of excitable cells come in a large variety of versions; see (4) for several hundred examples. The simplest possible model is just a passive current of the form $I_{\text{ion}} = \text{const} \cdot v$, followed by a third order polynomial model. More realistic models tend to be more complex and are usually written on the form

$$I_{\text{ion}} = \sum_{i=1}^{N} I_i, \tag{1.29}$$

given in μA/cm^2. Here, the individual currents can usually be written on the form $I_i = I_i(v, s)$, where v denotes the membrane potential, given by $u_i - u_e$, and s denotes gating variables and ionic concentrations. The celebrated model of the action potential of a neuron presented by Hodgkin and Huxley (see (14)) can be written on this form, and so can the first model of a cardiac cell presented by Nobel (25). A comprehensive and readable introduction to models of the membrane ionic currents is given in the survey (27).

Correspondingly, the ionic currents through gap junctions between neighboring cells are often modeled by a simple passive model of the form $I_{\text{gap}} = \text{const} \cdot w$. More detailed models of voltage-dependent gap junction dynamics have also been introduced (see e.g., (10; 35)).

1.2.6 Summary of the Model Equations

In summary, the EMI model for a single cell surrounded by an extracellular domain (as illustrated in Figure 1.1) is given by the equations (1.7), (1.8), (1.17), (1.22) and (1.25), that is

$$\nabla \cdot \sigma_i \nabla u_i = 0 \qquad \text{in } \Omega_i, \tag{1.30}$$

$$\nabla \cdot \sigma_e \nabla u_e = 0 \qquad \text{in } \Omega_e, \tag{1.31}$$

$$\sigma_e \nabla u_e \cdot \mathbf{n}_e = -\sigma_i \nabla u_i \cdot \mathbf{n}_i \equiv I_m \qquad \text{at } \Gamma, \tag{1.32}$$

$$v = u_i - u_e \qquad \text{at } \Gamma, \tag{1.33}$$

$$\frac{\partial v}{\partial t} = \frac{1}{C_m}(I_m - I_{\text{ion}}) \qquad \text{at } \Gamma, \tag{1.34}$$

where u_i, u_e and v are the intracellular, extracellular and membrane potentials, respectively, typically given in mV. Moreover, σ_i and σ_e are the intracellular and extracellular conductivities, respectively (typically in mS/cm), C_m is the membrane capacitance (typically in μF/cm^2), and Γ denotes the cell membrane. The ionic currents through channels, pumps and exchangers at the membrane are denoted by I_{ion} and typically given in μA/cm^2.

If several cells are connected at intercalated discs, as illustrated for two cells in Figure 1.3, the system of equations must be extended to include equations for the currents between cells. For two cells, this extension consists of the equations

$$\sigma_i \nabla u_i^2 \cdot \mathbf{n}_i^2 = -\sigma_i \nabla u_i^1 \cdot \mathbf{n}_i^1 \equiv I_{1,2} \qquad \text{at } \Gamma_{1,2}, \tag{1.35}$$

$$u_i^1 - u_i^2 = w \qquad \text{at } \Gamma_{1,2}, \tag{1.36}$$

$$w_t = \frac{1}{C_{1,2}}(I_{1,2} - I_{\text{gap}}) \qquad \text{at } \Gamma_{1,2}, \tag{1.37}$$

where, as above, $\Gamma_{1,2}$ is the intercalated disc, $\mathbf{n}_i^1$ is the outward pointing normal vector of Ω_i^1, $\mathbf{n}_i^2$ is the outward pointing normal vector of Ω_i^2, and u_i^1 and u_i^2 are the intracellular potentials (typically in mV) of Ω_i^1 and Ω_i^2, respectively. Furthermore, $C_{1,2}$ is the specific capacitance of the intercalated disc (typically in μF/cm^2), and I_{gap} is the current through the gap junctions (typically in μA/cm^2).

1.3 Conclusion

In the present chapter, we have derived the EMI model. The EMI model predicts electrical potentials in cells with an explicit geometrical representation and thus allows for more detail than homogenized models of excitable tissue. In the next chapter (7, Chapter 2), the model will be extended by taking ion concentration in the extracellular and intracellular spaces into account. Numerical solutions of the EMI models will be presented in (19, Chapter 4), (23, Chapter 5) and (22, Chapter 6). In these chapters the readers will also be pointed to open software that can be used to solve the EMI model.

References

1. Agudelo-Toro A (2012) Numerical simulations on the biophysical foundations of the neuronal extracellular space. PhD thesis, Niedersächsische Staats-und Universitätsbibliothek Göttingen
2. Anastassiou CA, Perin R, Markram H, Koch C (2011) Ephaptic coupling of cortical neurons. Nature neuroscience 14(2):217–223
3. Buccino A, Kuchta M, Jæger KH, Ness T, Berthet P, Mardal KA, Cauwenberghs G, Tveito A (2019) How does the presence of neural probes affect extracellular potentials? Journal of Neural Engineering 16:026030
4. Cuellar AA, Lloyd CM, Nielsen PF, Bullivant DP, Nickerson DP, Hunter PJ (2003) An overview of CellML 1.1, a biological model description language. Simulation 79(12):740–747
5. Einevoll GT (2006) Mathematical modeling of neural activity. In: Dynamics of Complex Interconnected Systems: Networks and Bioprocesses, Springer, pp 127–145
6. Einevoll GT, Kayser C, Logothetis NK, Panzeri S (2013) Modelling and analysis of local field potentials for studying the function of cortical circuits. Nature Reviews Neuroscience 14(11):770
7. Ellingsrud AJ, Daversin-Catty C, Rognes ME (2020) A cell-based model for ionic electrodiffusion in excitable tissue. In: Tveito A, Mardal KA, Rognes ME (eds) Modeling excitable tissue - The EMI framework, Simula Springer Notes in Computing, SpringerNature
8. Franzone PC, Pavarino LF, Scacchi S (2014) Mathematical cardiac electrophysiology, vol 13. Springer
9. Griffiths DJ (1989) Introduction to electrodynamics, 2nd edn. Prentice Hall
10. Henriquez AP, Vogel R, Muller-Borer BJ, Henriquez CS, Weingart R, Cascio WE (2001) Influence of dynamic gap junction resistance on impulse propagation in ventricular myocardium: a computer simulation study. Biophysical Journal 81(4):2112–2121
11. Henriquez CS, Ying W (2009) The bidomain model of cardiac tissue: from microscale to macroscale. In: Cardiac Bioelectric Therapy, Springer, pp 401–421
12. Herz AV, Gollisch T, Machens CK, Jaeger D (2006) Modeling single-neuron dynamics and computations: a balance of detail and abstraction. Science 314(5796):80–85
13. Hille B (2001) Ion channels of excitable membranes, vol 507. Sinauer Sunderland, MA
14. Hodgkin AL, Huxley AF (1952) A quantitative description of membrane current and its application to conduction and excitation in nerve. The Journal of Physiology 117(4):500–544
15. Holt GR (1998) A critical reexamination of some assumptions and implications of cable theory in neurobiology. PhD thesis, California Institute of Technology
16. Holt GR, Koch C (1999) Electrical interactions via the extracellular potential near cell bodies. Journal of computational neuroscience 6(2):169–184
17. Jæger KH (2019) Cell-based mathematical models of small collections of excitable cells. PhD thesis, University of Oslo

18. Jæger KH, Edwards AG, McCulloch A, Tveito A (2019) Properties of cardiac conduction in a cell-based computational model. PLoS computational biology 15(5):e1007042
19. Jæger KH, Hustad KG, Cai X, Tveito A (2020) Operator splitting and finite difference schemes for solving the emi model. In: Tveito A, Mardal KA, Rognes ME (eds) Modeling excitable tissue - The EMI framework, Simula Springer Notes in Computing, SpringerNature
20. Keener J, Sneyd J (2010) Mathematical physiology. Springer Science & Business Media
21. Kucera JP, Rohr S, Kleber AG (2017) Microstructure, cell-to-cell coupling, and ion currents as determinants of electrical propagation and arrhythmogenesis. Circulation: Arrhythmia and Electrophysiology 10(9):e004665
22. Kuchta M, Mardal KA (2020) Iterative solvers for cell-based emi models. In: Tveito A, Mardal KA, Rognes ME (eds) Modeling excitable tissue - The EMI framework, Simula Springer Notes in Computing, SpringerNature, pp 0–100
23. Kuchta M, Mardal KA, Rognes ME (2020) Solving the emi equations using finite element methods. In: Tveito A, Mardal KA, Rognes ME (eds) Modeling excitable tissue - The EMI framework, Simula Springer Notes in Computing, SpringerNature
24. Lin J, Keener JP (2010) Modeling electrical activity of myocardial cells incorporating the effects of ephaptic coupling. Proceedings of the National Academy of Sciences 107(49):20935–20940
25. Noble D (1962) A modification of the Hodgkin–Huxley equations applicable to purkinje fibre action and pacemaker potentials. The Journal of Physiology 160(2):317–352
26. Qu Z, Hu G, Garfinkel A, Weiss JN (2014) Nonlinear and stochastic dynamics in the heart. Physics Reports 543(2):61–162
27. Rudy Y (2012) From genes and molecules to organs and organisms: heart. Comprehensive Biophysics pp 268–327
28. Spach MS, Heidlage JF, Barr RC, Dolber PC (2004) Cell size and communication: role in structural and electrical development and remodeling of the heart. Heart Rhythm 1(4):500–515
29. Sperelakis N, McConnell K (2002) Electric field interactions between closely abutting excitable cells. IEEE Engineering in Medicine and Biology Magazine 21(1):77–89
30. Sterratt D, Graham B, Gillies A, Willshaw D (2011) Principles of computational modelling in neuroscience. Cambridge University Press
31. Stinstra JG, Roberts SF, Pormann JB, MacLeod RS, Henriquez CS (2006) A model of 3D propagation in discrete cardiac tissue. In: Computers in Cardiology, 2006, IEEE, pp 41–44
32. Stinstra JG, Henriquez CS, MacLeod RS (2009) Comparison of microscopic and bidomain models of anisotropic conduction. In: Computers in Cardiology, 2009, IEEE, pp 657–660
33. Trayanova NA (2011) Whole-heart modeling: applications to cardiac electrophysiology and electromechanics. Circulation Research 108(1):113–128
34. Tveito A, Jæger KH, Lines GT, Paszkowski Ł, Sundnes J, Edwards AG, Mäki-Marttunen T, Halnes G, Einevoll GT (2017) An evaluation of the accuracy of classical models for computing the membrane potential and extracellular potential for neurons. Frontiers in Computational Neuroscience 11:27
35. Weinberg SH (2017) Ephaptic coupling rescues conduction failure in weakly coupled cardiac tissue with voltage-gated gap junctions. Chaos: An Interdisciplinary Journal of Nonlinear Science 27(9):093908